

APOGEE-2 Discovery of a Large Population of Relatively High-Metallicity Globular Cluster Debris

JOSÉ G. FERNÁNDEZ-TRINCADO,^{1,2} TIMOTHY C. BEERS,³ ANNA. B. A. QUEIROZ,⁴ CRISTINA CHIAPPINI,^{4,5}
DANTE MINNITI,^{6,7} BEATRIZ BARBUY,⁸ STEVEN R. MAJEWSKI,⁹ MARIO ORTIGOZA-URDANETA,² CHRISTIAN MONI BIDIN,¹
ANNIE C. ROBIN,¹⁰ EDMUNDO MORENO,¹¹ LEONARDO CHAVES-VELASQUEZ,^{12,13,14} SANDRO VILLANOVA,¹⁵
RICHARD R. LANE,¹⁶ KAIKE PAN,¹⁷ AND DMITRY BIZYAEV^{17,18}

¹*Instituto de Astronomía, Universidad Católica del Norte, Av. Angamos 0610, Antofagasta, Chile*

²*Instituto de Astronomía y Ciencias Planetarias, Universidad de Atacama, Copayapu 485, Copiapó, Chile*

³*Department of Physics and JINA Center for the Evolution of the Elements, University of Notre Dame, Notre Dame, IN 46556, USA*

⁴*Leibniz-Institut für Astrophysik Potsdam (AIP), An der Sternwarte 16, 14482 Potsdam, Germany*

⁵*Laboratório Interinstitucional de e-Astronomia - LIneA, Rua Gal. José Cristino 77, Rio de Janeiro, RJ - 20921-400, Brazil*

⁶*Depto. de Cs. Físicas, Facultad de Ciencias Exactas, Universidad Andrés Bello, Av. Fernández Concha 700, Las Condes, Santiago, Chile*

⁷*Vatican Observatory, V-00120 Vatican City State, Italy*

⁸*Universidade de São Paulo, IAG, Rua do Matão 1226, Cidade Universitária, São Paulo 05508-900, Brazil*

⁹*Department of Astronomy, University of Virginia, Charlottesville, VA 22904, USA*

¹⁰*Institut Utinam, CNRS UMR 6213, Université Bourgogne-Franche-Comté, OSU THETA Franche-Comté, Observatoire de Besançon, BP 1615, 25010 Besançon Cedex, France*

¹¹*Instituto de Astronomía, Universidad Nacional Autónoma de México, Apdo. Postal 70264, México D.F., 04510, México*

¹²*Instituto de Radioastronomía y Astrofísica, Universidad Nacional Autónoma de México, Apdo. postal 3-72, Morelia Michoacán, 58089, Mexico*

¹³*Astronomical Observatory, Universidad de Nariño, Sede VIIS, Avenida Panamericana, Pasto, Nariño, Colombia*

¹⁴*Departamento de Física de la Universidad de Nariño, Torobajo Calle 18 Carrera 50, Pasto, Narino, Colombia*

¹⁵*Departamento de Astronomía, Casilla 160-C, Universidad de Concepción, Concepción, Chile*

¹⁶*Centro de Investigación en Astronomía, Universidad Bernardo O'Higgins, Avenida Viel 1497, Santiago, Chile*

¹⁷*Apache Point Observatory and New Mexico State University, P.O. Box 59, Sunspot, NM, 88349-0059, USA*

¹⁸*Sternberg Astronomical Institute, Moscow State University, Moscow*

ABSTRACT

We report the discovery of a new, chemically distinct population of relatively high-metallicity ($[\text{Fe}/\text{H}] > -0.7$) red giant stars with super-solar $[\text{N}/\text{Fe}]$ ($\gtrsim +0.75$) identified within the bulge, disk, and halo of the Milky Way. This sample of stars was observed during the second phase of the Apache Point Observatory Galactic Evolution Experiment (APOGEE-2); the spectra of these stars are part of the seventeenth Data Release (DR 17) of the Sloan Digital Sky Survey. We hypothesize that this newly identified population was formed in a variety of progenitors, and are likely made up of either fully or partially destroyed metal-rich globular clusters, which we refer to as Globular Cluster Debris (GCD), identified by their unusual photospheric nitrogen abundances. It is likely that some of the GCD stars were probable members of the *Gaia*-Enceladus-Sausage accretion event, along with clusters formed in situ.

Keywords: Stellar abundances (1577); Red giant stars (1368); Globular star clusters (656)

1. INTRODUCTION

It is well known that the Milky Way (MW) is populated by a great variety (~ 170) of ancient globular clusters (GCs)–(Gratton et al. 2004; Vasiliev & Baum-

gardt 2021; Baumgardt & Vasiliev 2021, and references therein), and perhaps a hundred new low-luminosity candidates uncovered in the inner Galaxy (Minniti et al. 2017).

The MW GCs measured so far span a wide range of metallicities, above the so-called “metallicity floor” at $[\text{Fe}/\text{H}] = -2.5$, with only two cases that have metallicities close to this value, VVV CL001 at $[\text{Fe}/\text{H}] = -2.45$

(Fernández-Trincado et al. 2021) and ESO280–SC06 at $[\text{Fe}/\text{H}] = -2.48$ (Simpson 2018).

While many of these systems have long survived, a handful of unique field stars with chemical patterns differing from the typical patterns observed in the MW and other Local Group galaxies suggest that many of the surviving and destroyed GCs have deposited part or all of their stellar content into the bulge, disk, and halo of the MW (see, e.g., Nissen & Schuster 2010; Fernández-Trincado et al. 2016, 2017, 2019a; Hanke et al. 2020; Wan et al. 2020).

On the metal-rich end, a handful of GCs have been found to exhibit metallicities very near solar metallicity, such as Pal 10 (Harris 2010). Motivated by the prospects of unearthing new examples of such GC debris, we have searched for the presence of relatively high-metallicity ($[\text{Fe}/\text{H}] \gtrsim -0.7$) GC debris throughout the MW within the footprint of the APOGEE-2 survey.

In this Letter, we report the discovery of a significant population of high-metallicity Globular Cluster Debris (GCD) stars within the bulge, disk, and halo of the MW likely associated with small pieces of destroyed GCs and identified by their unusual nitrogen abundances.

2. DATA

We employ interim data from the seventeenth data release (DR 17) of the second generation of the Apache Point Observatory Galactic Evolution Experiment (APOGEE-2) survey (Majewski et al. 2017), which is one of the programs of the Sloan Digital Sky Survey (SDSS-IV; Blanton et al. 2017). The APOGEE instruments are high-resolution ($R \sim 22,500$), near-infrared (collecting $\sim 2/3$ of the H -band: 15145–16960 Å; vacuum wavelengths) spectrographs (Wilson et al. 2019) that operate on the Sloan 2.5m telescope (Gunn et al. 2006) at Apache Point Observatory (APOGEE-2N) and on the Irénée du Pont 2.5m telescope (Bowen & Vaughan 1973) at Las Campanas Observatory (APOGEE-2S).

As of January 2021, the dual APOGEE instruments have observed more than 700,000 stars across the MW. Zasowski et al. (2017), Beaton et al. (2021), and Santana et al. (2021) provide a detailed overview of the targeting strategy of the APOGEE-2 survey. Spectra are reduced as described in Nidever et al. (2015), and analyzed using the APOGEE Stellar Parameters and Chemical Abundance Pipeline (García Pérez et al. 2016, hereafter ASPCAP/APOGEE-2) and the libraries of synthetic spectra described in Zamora et al. (2015). The accuracy and precision of the atmospheric parameters and chemical abundances are extensively analyzed in Holtzman et al. (2018), while details regarding the customized H -band

line list are fully described in Shetrone et al. (2015) and Smith et al. (2021).

3. SAMPLE SELECTION

We restrict our sample to giant stars ($\log g < 3.6$) that have been flagged as `ASPCAPFLAG=0`, `ALFE_FLAG=0`, `NFE_FLAG=0`, and have a spectral signal-to-noise ratio (SNR) larger than 70. Our sample is also restricted to $3200 \text{ K} < T_{\text{eff}} < 5500 \text{ K}$, in order to avoid large uncertainties in $[\text{N}/\text{Fe}]$ due to the weakness of the $^{12}\text{C}^{14}\text{N}$, $^{12}\text{C}^{16}\text{O}$, and ^{16}OH molecules, which together are required to determine the nitrogen, oxygen, and carbon abundances. Moreover, because we are interested in searching for relatively high-metallicity ($-0.7 < [\text{Fe}/\text{H}] \lesssim -0.1$) stellar debris with possible GC origin, we restrict our analysis to relatively carbon-poor stars, $[\text{C}/\text{Fe}] \lesssim +0.15$ (see Martell et al. 2016; Schiavon et al. 2017; Fernández-Trincado et al. 2019b, 2020a,b,d, for a discussion), because such stars are typically found in GCs (see e.g., Mészáros et al. 2020), and at the same time minimize potential contamination by objects such as CH stars (Karinkuzhi & Goswami 2015), whose surface abundances may have been modified by mass-transfer from low-mass companion AGB stars (Karinkuzhi & Goswami 2015). The cuts above return a data set of 143,141 unique sources, after removing duplicate entries. This sample has been divided in several main populations as described in next section.

4. POTENTIAL HIGH-METALLICITY GLOBULAR CLUSTER DEBRIS

As nitrogen enrichment in GCs is even larger than what is possible/expected from pure mixing processes (see, e.g., Shetrone et al. 2019) occurring in non-cluster stars, we start by evaluating the chemical species (N and Al) that typically participate in the characteristic GC abundance patterns over a wide range of metallicities (see, e.g., Mészáros et al. 2020). In the following, we describe our two-step selection of outliers in the $[\text{N}/\text{Fe}]$ – $[\text{Al}/\text{Fe}]$ space.

First, we carried out a population analysis in the $[\text{Al}/\text{Fe}]$ – $[\text{N}/\text{Fe}]$ plane using the k -means clustering approach, as described in Ivezić et al. (2014). The k -means clustering algorithm revealed the existence of a significant population of stars that is separated relatively cleanly from the MW field stars approximately between $\{[\text{N}/\text{Fe}], [\text{Al}/\text{Fe}]\} = \{+0.75, -0.05\}$ and $\{+1.55, +1.1\}$, and have been found to be $> 4\sigma$ above the typical MW field stars in the $[\text{Fe}/\text{H}]$ – $[\text{N}/\text{Fe}]$ plane at fixed metallicity. After removing 50 well-studied APOGEE-2 GC stars (Mészáros et al. 2020), and ~ 145 poten-

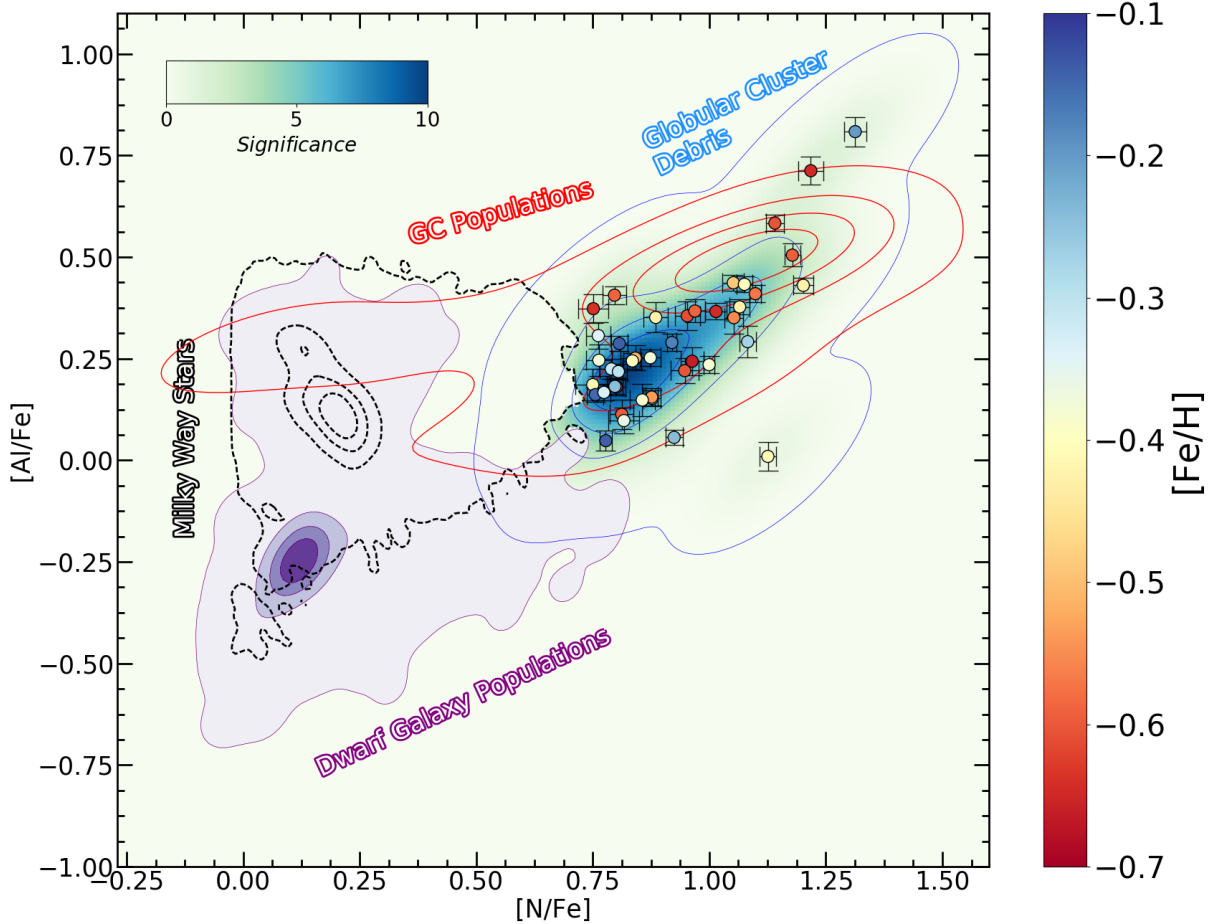


Figure 1. Distribution of $[Al/Fe]$ vs. $[N/Fe]$ for all stars used in our analysis, which all have been chosen to be of high metallicity ($[Fe/H] > -0.7$). Also included are KDE models and contours showing the density of objects belonging to the MW Stars (black contours), Dwarf Galaxy Populations (purple contours), GC Populations (red contours), and the newly identified population—the GCD stars (blue contours and circle symbols). Stars among the GCD are also overlaid with dot symbols with color-coding based on their $[Fe/H]$. The background green to blue color highlighted by the inset bar indicate the significance of the GCD stars as compared to the background density level.

tial GCs candidates¹ not analyzed in Mészáros et al. (2020). Thus, the final sample was reduced to a total of 42 unique stars, marked with circles in Figure 1. There are no known GCs within an angular separation of 0.5° from these stars.

For comparison, with our relatively high-metallicity outliers (potential GCDs), we define and include in Figure 1 four main populations of similar metallicity ($[Fe/H] > -0.7$) stars: MW stars (140,270 source in the thin and thick disk as well as likely metal-rich halo

stars), confirmed dwarf galaxy stars (2,634 sources in the Sagittarius, and the Large and Small Magellanic Clouds) from Gaia Collaboration et al. (2018) with ASPCAP/APOGEE-2 DR 17 abundances (dwarf galaxy populations), and relatively high-metallicity GC stars (50 sources) from Mészáros et al. (2020) having ASPCAP-measured abundances in DR17. We ran a Kernel Density Estimation (KDE) model over the stars in every population, as shown in Figure 1. As can be appreciated from inspection of this Figure 1, the MW stars and dwarf galaxy populations lie below $[N/Fe] \lesssim +0.75$ over a wide range of $[Al/Fe]$ abundance ratios, and well below $[Al/Fe] \lesssim +0.5$. In contrast, the relatively high-metallicity GCs span a range in $[N/Fe]$, which is much wider than that of the MW and dwarf galaxy popula-

¹ These sources were not included in our analysis, as the potential progenitors are primarily located in regions heavily reddened which requires a more exhaustive treatment of their atmospheric parameters and elemental abundances.

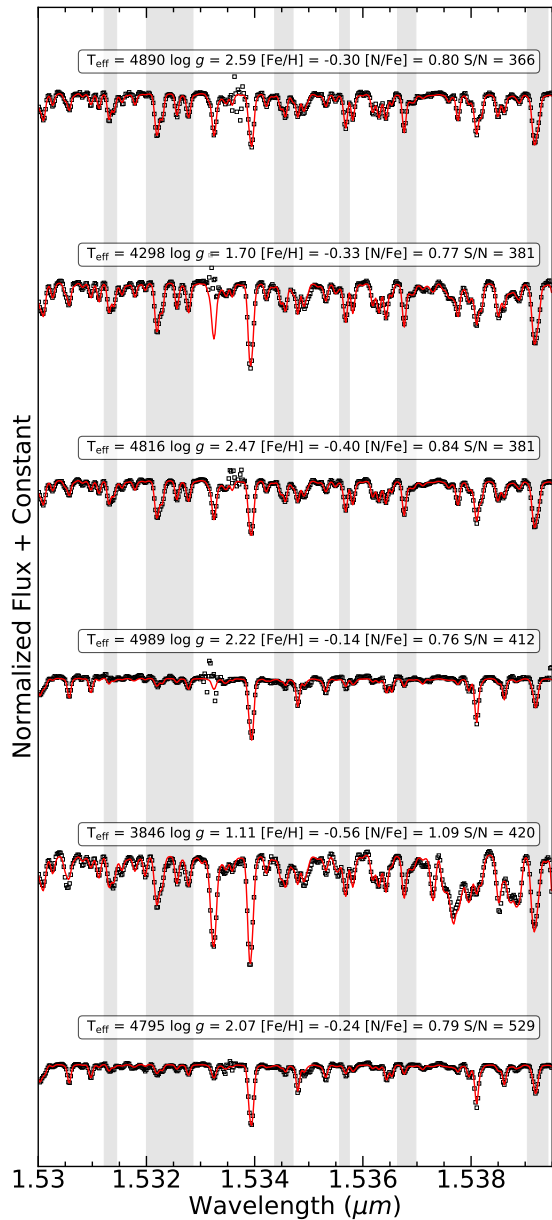


Figure 2. High-resolution near-IR H -band spectra (black empty squares) of six arbitrary stars identified as potential members of the GCD population, covering a small portion of the observed spectral regions around the $^{12}\text{C}^{14}\text{N}$ band (grey bands). The best-fit models based on the *ASPCAP*/*APOGEE-2* spectral synthesis are superposed (red lines).

tions, and exhibits $[\text{Al}/\text{Fe}]$ abundance ratios from the solar level to $[\text{Al}/\text{Fe}] < +1.0$.

Figure 1 also shows some main characteristics of the newly identified GCD population. For instance, Figure 1 reveal that the GCD clearly occupies the locus dominated by the nitrogen enriched ($[\text{N}/\text{Fe}] \gtrsim +0.7$) GC pop-

ulations, suggesting that GCD stars may have formed in different sites than typical MW stars, unless they were part of systems with contribution from “spinstars” (Frischnecht et al. 2016), which would alternatively explain the anomalous abundance signature. Close inspection of Figure 1 also reveals a fairly clear clump of potential GCD stars that are not located in the main bulk of the KDE of the MW stars or dwarf galaxy populations, exceeding the background level by a factor of more than 10. This suggests the existence of a statistically significant newly discovered stellar population of potential GCD stars in the relatively high-metallicity regime.

The $[\text{N}, \text{Al}/\text{Fe}]$ -peak is clearly visible at $([\text{N}/\text{Fe}], [\text{Al}/\text{Fe}]) \gtrsim (+0.75, +0.0)$ in Figure 1; a set of contour lines is provided as a visual aid. The statistical significance of the detection of newly identified GCD stars confirms and reinforces the existence of a newly discovered, relatively high-metallicity stellar sub-population whose origin is different from that of MW stars, and clearly well-separated from the MW and dwarf galaxy stellar systems.

Figure 2 shows examples of the typical high-S/N *APOGEE-2* DR 17 spectra of arbitrarily selected stars belonging to the GCD population, covering a small portion of the observed spectral regions around the remarkably strong $^{12}\text{C}^{14}\text{N}$ lines, along with corresponding best-fit models from the *ASPCAP*/*APOGEE-2* spectral synthesis. It is clear that the *ASPCAP* analysis is performing well on these stars, in particular, in the regions of the cyanogen bands.

Figure 3 shows the chemical-abundance patterns of selected *APOGEE-2* DR 17 chemical species for the relatively high-metallicity GCD stars compared to those for the MW stars, dwarf galaxy populations, and GC populations. While the GCD stars largely follow the expected chemical enrichment of the relatively high-metallicity GC populations, we cannot rule out possible contamination from the incidence of variable stars or mass-transfer events in our sample, which could be responsible for producing the anomalous abundance variations (primarily with N and Al) observed in this relatively high-metallicity regime.

Even though our *APOGEE-2* DR 17 data do not provide any strong evidence for variability in radial velocity over the period of the *APOGEE-2* DR 17 observations, we identify one star in our sample (2M06410076–6926199) with $[\text{N}/\text{Fe}] > +0.87$, $[\text{Al}/\text{Fe}] \sim +0.16$, and $[\text{Mg}/\text{Fe}] \sim +0.34$ that has been classified (with a 97% of probability) as a semi-regular variable (likely a highly evolved AGB star) with a period of 17.17 days and low amplitude (0.08 mag) in the *ASAS-SN* Catalog (Jayasinghe et al. 2021). Unfortunately, the

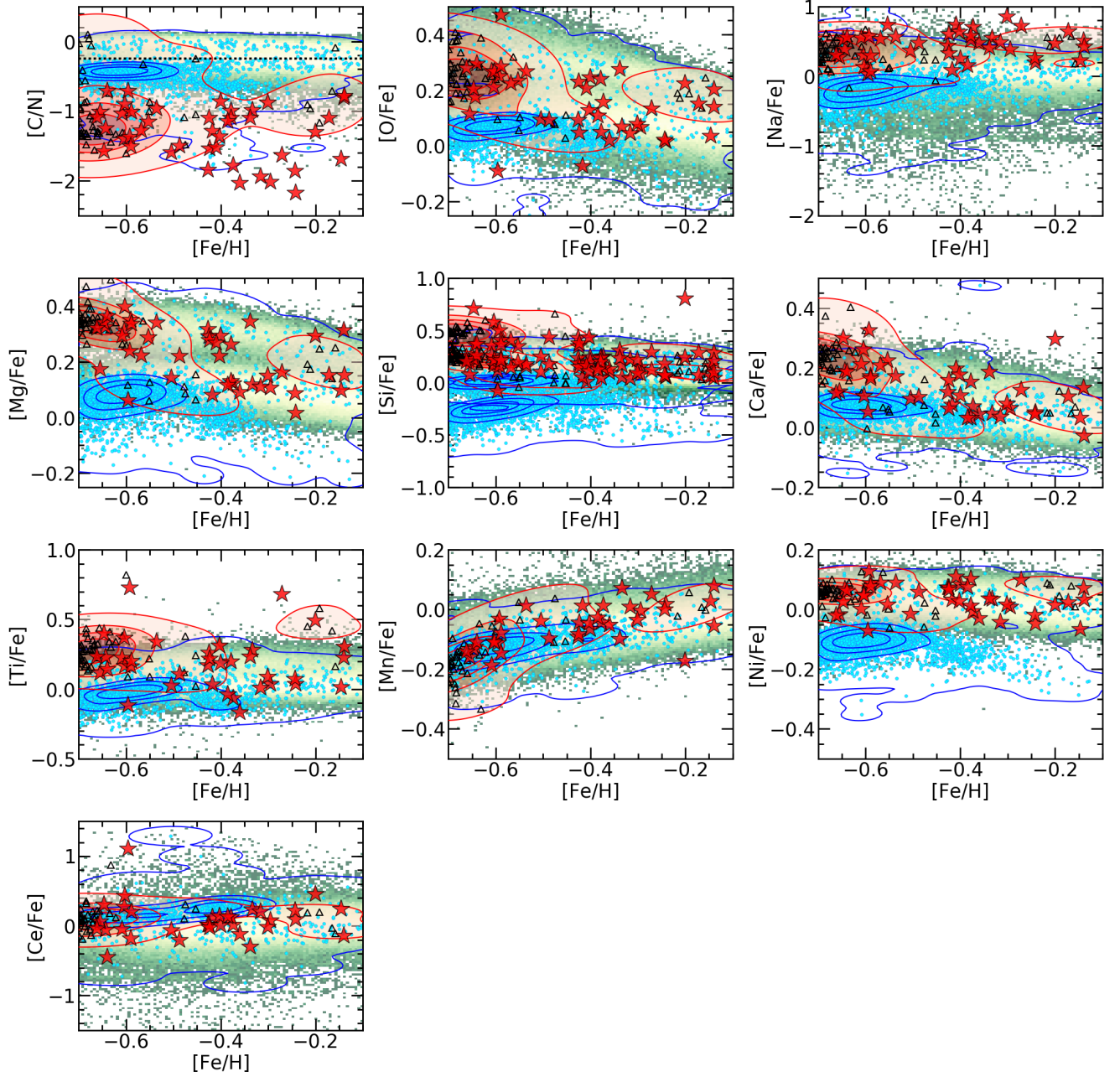


Figure 3. Chemical-abundance patterns of selected elements for the relatively high-metallicity GCD population (red filled stars) compared to the MW stars (green 2D density histogram), dwarf galaxy populations (cyan circles and blue contours), and GC populations (black empty triangles and red contours). The black dotted line highlighted in the [Fe/H]–[C/N] plane indicates the limit above which extra-mixing episodes are expected to take place (see, e.g., Shetrone et al. 2019).

s-process ($[\text{Ce}/\text{Fe}]$) abundance ratio for this star is not determined by the ASPCAP/APOGEE-2 pipeline, which makes it difficult to provide a rough estimate of the mass of the presumed AGB.

Figure 3 also reveals that our sample lies well below $[\text{C}/\text{N}] \sim -0.25$, which indicates that the chemical anomalies observed in our sample are unlikely to be affected by extra-mixing processes (see, e.g., Shetrone et al. 2019). This suggests that whatever process is responsible for the abundances observed in the GCD population is similar to that associated with the production of this signature for relatively high-metallicity GCs.

5. DYNAMICAL PROPERTIES OF SELECTED GLOBULAR CLUSTER DEBRIS STARS

We study the kinematics and dynamical properties of our sample by making use of the GravPot16_VAC_DR17 Value Added Catalog² (Fernández-Trincado et al., in preparation) of ensemble orbits integrated over a 3 Gyr timespan with the GravPot16³ model (Fernández-Trincado et al. 2020c). For the orbit computations we assumed a bar pattern speed of $41 \pm 10 \text{ km s}^{-1} \text{ kpc}^{-1}$ (Sanders et al. 2019). We note that our model has some limitations in the processes considered; e.g., secular changes in the adopted MW potential as well as dynamical friction are not included.

The orbit calculations were performed by adopting a simple Monte Carlo approach that considers the errors of the observables. The resulting values and their errors were taken as the 16th, 50th, and 84th percentiles from the generated distributions. Heliocentric distances were estimated with the StarHorse code (see, e.g., Queiroz et al. 2018, 2020a,b), proper motions are from *Gaia* EDR 3 (Gaia Collaboration et al. 2021), and radial velocities are provided from the APOGEE-2 DR 17 database. Figure 4 shows the resulting orbital elements for the 32 out of 42 stars in our sample that have a *Gaia* re-normalized unit weight error (RUWE) less than 1.4 (indicating the high quality of their astrometric solutions).

We find that the great majority of the stars (27 out of 32) in our sample tagged as GCD members exhibit prograde orbits, with the exception of five stars. Among those five, four exhibit the unusual behavior of orbits that change their sense of motion from prograde to retrograde (P–R orbits) during the integration time, and one star that is in retrograde motion.

We also find that three of the stars with P–R orbits, the star on a retrograde orbit, and one star with

a prograde orbit have kinematical properties compatible with the position of the *Gaia*-Enceladus-Sausage (GES) accretion event (Belokurov et al. 2018), as can be appreciated from inspection of Figure 4(a). Like GES stars, these GES candidates in our sample have radial/eccentric orbits. The stars in the P–R configurations are on bulge-like orbits ($r_{apo} < 3.5 \text{ kpc}$) with small vertical excursions above the Galactic plane ($Z_{\max} < 2.5 \text{ kpc}$), while the retrograde star exhibits a radial and high-eccentricity, halo-like orbit, with large vertical excursions from the Galactic plane ($Z_{\max} > 9 \text{ kpc}$); see Figures 4(b) and (c). Strikingly, three of the stars in our sample with GES-like kinematics have $[\text{Fe}/\text{H}] > -0.38$, and are strongly enriched in nitrogen ($[\text{N}/\text{Fe}] \gtrsim +0.77$), with $[\text{Al}/\text{Fe}]$ abundance ratios ranging from $+0.05$ to $+0.29$, and sodium enrichment above $[\text{Na}/\text{Fe}] = +0.27$. Thus, the very peculiar dynamics of these stars, combined with the enrichment levels of their constituent chemical elements, make these five stars potential members of dissipated metal-rich ($[\text{Fe}/\text{H}] > -0.7$) GCs that are likely associated with the progenitor GES dwarf galaxy.

Figure 4(a) also reveals that the majority of stars on prograde orbits exhibit disk-like kinematics, with typical orbital eccentricities below $e = 0.6$, and small vertical excursions below the Galactic plane ($Z_{\max} \lesssim 3.0 \text{ kpc}$), with a few exceptions on halo-like orbits (and $Z_{\max} > 3.0 \text{ kpc}$). The dark-gray shadow region in Figures 4(b) and (c) reveals that stars (13 out of the 32) with lower eccentricities ($e \lesssim 0.4$) exhibit a peak in their perigalactocentric distances between 4 and 9 kpc, apogalactocentric distances between ~ 8.5 and 12 kpc, and are on in-plane orbits with $Z_{\max} < 0.5 \text{ kpc}$; this places these stars on disk-like orbits very near the Solar Neighborhood, with radial excursions reaching the co-rotation radius. The stars with prograde orbits outside these dynamical limits are likely on inner-halo-like orbits.

Our dynamical analysis clearly reveals that there are at least four different dynamical families of stars represented within the GCD sample and suggesting a variety of origin scenarios: (*i*) the group of stars that lives in bulge-like orbits likely ejected from in situ disk/bulge GCs; (*ii*) the stars dynamically lost to the inner-most parts of the MW, from a massive accreted system, such as the GES dwarf galaxy; (*iii*) stars in the Solar Neighborhood with in-plane orbits; and (*iv*) stars with halo-like orbits. The presence of four distinctly different dynamical groups among the GCD sample suggests that there is not a single common origin for these stars and their origins are not like those of typical MW populations. We conclude that, if metal-rich GCs are responsible for these chemically unique stars, then there should

² https://internal.sdss.org/dr17/datamodel/files/APOGEE_GRAVPOT16/GravPot16_VAC_DR17.html

³ <https://gravpot.utinam.cnrs.fr>

be several groups of GCs contributing to the GCD population, e.g., those formed in-situ and those with an extragalactic origin (see, e.g., [Massari et al. 2019](#)).

6. CONCLUSIONS

We report on the discovery of a large population of relatively high-metallicity ($-0.7 < [\text{Fe}/\text{H}] < -0.1$) Globular Cluster Debris (GCD) stars identified in the interim data from the seventeenth data release of the APOGEE-2 Survey.

The newly identified GCD stars are strongly enriched in nitrogen ($[\text{N}/\text{Fe}] \gtrsim +0.75$), and chemically distinct from MW and dwarf galaxy stars in almost all the chemical species examined so far, but with chemical patterns similar to those found in GC populations of comparable metallicity. We find that most of the relatively high-metallicity GCD stars lie on bulge- (stars with P-R orbits), disk- and halo-like orbits, and are likely part of the cumulative effect of many events, including partially or completely dissolved disk/bulge GCs of relative high metallicity, and/or dissolved GCs stars ejected from massive accretion events, such as the *Gaia*-Enceladus-Sausage. Stars in our sample were mostly identified within the bulge, disk (likely the thick disk) and halo of the MW.

The presence of a semi-regular variable (likely an AGB star) in our sample makes it possible that there is some contamination in our sample by variable stars and/or mass-transfer events, which could explain part of the chemically anomalous patterns at relatively high-metallicity. Future, long-term radial-velocity monitoring of our sample would naturally be the best course to establish the number of such sources formed through the binary or pulsating-star channels.

Finally, we conclude that, whatever process is responsible for the origin of the GCD stars, it is similar to that associated with the production of the unusual chemical-abundance patterns in relatively high-metallicity GCs.

7. DATA AVAILABILITY

The observational data underlying this article are from *Gaia* EDR3, and from the 17th data release of the Sloan Digital Sky Survey (SDSS-IV), which are proprietary and will later be made publicly available. A short list of the APOGEE-Ids of all the potential members of the High-Metallicity Globular Cluster Debris can be found in the Table 1.

We thank the anonymous referee for helpful comments that greatly improved the paper. T.C.B. acknowledges partial support for this work from grant PHY 14-30152: Physics Frontier Center / JINA Center for the Evolution of the Elements (JINA-CEE), awarded by the

Table 1. APOGEE-Ids of the High-Metallicity Globular Cluster Debris Stars

APOGEE-Ids	APOGEE-Ids
2M17372753-0425598	2M06410076-6926199
2M05254390-0237519	2M06202897-6558047
2M05495421+0043416	2M07084597-6227180
2M11173689+0645217	2M05120630-5913438
2M22534888+0919004	2M06040390-5600065
2M08280055+1036106	2M08234846-4918149
2M04392467+2348469	2M17571419-3328194
2M16051430+2801104	2M08120643-3320409
2M19261583+3653131	2M17255366-3208304
2M02073982+3707297	2M18022530-2928338
2M10392171+3828495	2M17480068-2922069
2M05294163+3942524	2M17433446-2842533
2M19233926+4003386	2M17372741-2816560
2M19442885+4354544	2M17173130-2728590
2M06383118+4646336	2M17305251-2651528
2M23065670+4724235	2M16485601-2522202
2M21070345+4733270	2M18341668-2333440
2M22050390+5500110	2M17441535-2227514
2M08513911+5550206	2M06301992-1604284
2M12595431+5811394	2M11014631-1051279
2M03521331+6755389	2M18531386-0942286

US National Science Foundation. D.M. is supported by the BASAL Center for Astrophysics and Associated Technologies (CATA) through grant AFB 170002, and by project FONDECYT Regular No. 1170121. B.B. acknowledge partial financial support from FAPESP, CNPq, and CAPES - Finance Code 001. L.C.V acknowledges the support of the postdoctoral Fellowship of DGAPA-UNAM, México, and the Fondo Nacional de Financiamiento para la Ciencia, La Tecnología y la innovación “FRANCISCO JOSÉ DE CALDAS”, MIN-CIENCIAS, and the VIIS for the economic support of this research.

Funding for the Sloan Digital Sky Survey IV has been provided by the Alfred P. Sloan Foundation, the U.S. Department of Energy Office of Science, and the Participating Institutions. SDSS-IV acknowledges support and resources from the Center for High-Performance Computing at the University of Utah. The SDSS website is www.sdss.org.

SDSS-IV is managed by the Astrophysical Research Consortium for the Participating Institutions of the SDSS Collaboration including the Brazilian Participation Group, the Carnegie Institution for Science, Carnegie Mellon University, the Chilean Participation Group, the French Participation Group, Harvard

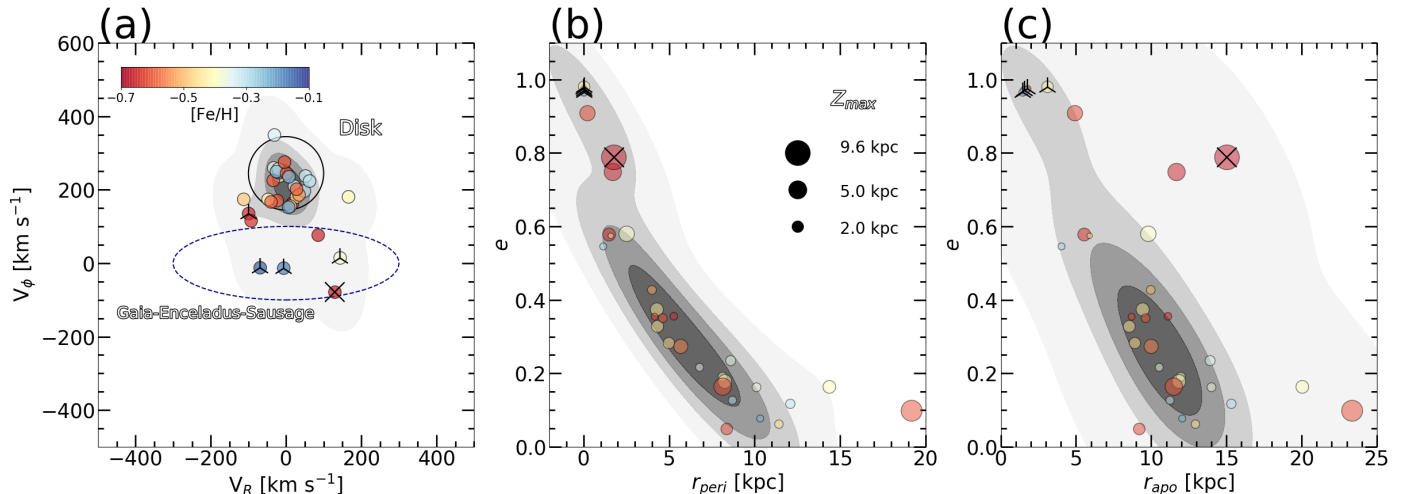


Figure 4. Kinematics and orbital-element properties of selected GCD stars. The color-coding of the symbols in the panels is based on their $[\text{Fe}/\text{H}]$, while the gray background shading represents the Kernel Density Estimation (KDE) model of the overlaid points. The distribution of the velocity component V_R vs. V_ϕ is shown in panel (a). The blue dashed line represents the approximate region for sources associated with the *Gaia*-Enceladus-Sausage in V_R vs. V_ϕ , based on Belokurov et al. (2018). The area occupied by disk-like stars is also highlighted with the black empty circle. The perigalactic and apogalactic distances, as a function of the orbital eccentricity, are shown in panels (b) and (c), respectively. The point sizes reflect their maximum vertical heights above the Galactic plane (Z_{max}), with decreasing size for decreasing Z_{max} . Three black points at 2, 5, and 9.6 kpc are provided as a visual aid. Black up-tick symbols mark the stars with P-R orbital configurations (see text), while the “X” symbol indicates the star with a retrograde orbit.

Smithsonian Center for Astrophysics, Instituto de Astrofísica de Canarias, The Johns Hopkins University, Kavli Institute for the Physics and Mathematics of the Universe (IPMU) / University of Tokyo, Lawrence Berkeley National Laboratory, Leibniz Institut für Astrophysik Potsdam (AIP), Max-Planck-Institut für Astronomie (MPIA Heidelberg), Max-Planck-Institut für Astrophysik (MPA Garching), Max-Planck-Institut für Extraterrestrische Physik (MPE), National Astronomical Observatory of China, New Mexico State University, New York University, the University of Notre Dame, Observatório Nacional / MCTI, The Ohio State University, Pennsylvania State University, Shanghai Astronomical Observatory, United Kingdom Participation Group, Universidad Nacional Autónoma de México, University of Arizona, University of Colorado Boulder, University of Oxford, University of Portsmouth, University of Utah, University of Virginia, University of Washington, University of Wisconsin, Vanderbilt Uni-

versity, and Yale University.

This work has made use of data from the European Space Agency (ESA) mission *Gaia* (<http://www.cosmos.esa.int/gaia>), processed by the *Gaia* Data Processing and Analysis Consortium (DPAC, <http://www.cosmos.esa.int/web/gaia/dpac/consortium>). Funding for the DPAC has been provided by national institutions, in particular the institutions participating in the *Gaia* Multilateral Agreement.

Simulations have been executed on HPC resources on the Cluster Supercomputer Atocatl from Universidad Nacional Autónoma de México (UNAM). The Geryon2 cluster housed at the Centro de Astro-Ingeniería UC was used for the calculations performed in this paper. The BASAL PFB-06 CATA, Anillo ACT-86, FONDEQUIP AIC-57, and QUIMAL 130008 provided funding for several improvements to the Geryon/Geryon2 cluster.

REFERENCES

- Baumgardt, H., & Vasiliev, E. 2021, *MNRAS*, 505, 5957
 Beaton, R. L., Oelkers, R. J., Hayes, C. R., et al. 2021, *ApJ*, in preparation
 Belokurov, V., Erkal, D., Evans, N. W., Koposov, S. E., & Deason, A. J. 2018, *MNRAS*, 478, 611
 Blanton, M. R., Bershady, M. A., Abolfathi, B., et al. 2017, *AJ*, 154, 28
 Bowen, I. S., & Vaughan, A. H., J. 1973, *ApOpt*, 12, 1430
 Fernández-Trincado, J. G., Beers, T. C., & Minniti, D. 2020a, *A&A*, 644, A83

- Fernández-Trincado, J. G., Beers, T. C., Minniti, D., et al. 2020b, *A&A*, 643, L4
- Fernández-Trincado, J. G., Beers, T. C., Tang, B., et al. 2019a, *MNRAS*, 488, 2864
- Fernández-Trincado, J. G., Chaves-Velasquez, L., Pérez-Villegas, A., et al. 2020c, *MNRAS*, 495, 4113
- Fernández-Trincado, J. G., Robin, A. C., Moreno, E., et al. 2016, *ApJ*, 833, 132
- Fernández-Trincado, J. G., Zamora, O., García-Hernández, D. A., et al. 2017, *ApJL*, 846, L2
- Fernández-Trincado, J. G., Beers, T. C., Placco, V. M., et al. 2019b, *ApJL*, 886, L8
- Fernández-Trincado, J. G., Beers, T. C., Minniti, D., et al. 2020d, *ApJL*, 903, L17
- Fernández-Trincado, J. G., Minniti, D., Souza, S. O., et al. 2021, *ApJL*, 908, L42
- Frischknecht, U., Hirschi, R., Pignatari, M., et al. 2016, *MNRAS*, 456, 1803
- Gaia Collaboration, Helmi, A., van Leeuwen, F., et al. 2018, *A&A*, 616, A12
- Gaia Collaboration, Brown, A. G. A., Vallenari, A., et al. 2021, *A&A*, 649, A1
- García Pérez, A. E., Allende Prieto, C., Holtzman, J. A., et al. 2016, *AJ*, 151, 144
- Gratton, R., Sneden, C., & Carretta, E. 2004, *ARA&A*, 42, 385
- Gunn, J. E., Siegmund, W. A., Mannery, E. J., et al. 2006, *AJ*, 131, 2332
- Hanke, M., Koch, A., Prudil, Z., Grebel, E. K., & Bastian, U. 2020, *A&A*, 637, A98
- Harris, W. E. 2010, arXiv e-prints, arXiv:1012.3224
- Holtzman, J. A., Hasselquist, S., Shetrone, M., et al. 2018, *AJ*, 156, 125
- Ivezić, Ž., Connelly, A. J., VanderPlas, J. T., & Gray, A. 2014, *Statistics, Data Mining, and Machine Learning in Astronomy*
- Jayasinghe, T., Kochanek, C. S., Stanek, K. Z., et al. 2021, *MNRAS*, 503, 200
- Karinkuzhi, D., & Goswami, A. 2015, *MNRAS*, 446, 2348
- Majewski, S. R., Schiavon, R. P., Frinchaboy, P. M., et al. 2017, *AJ*, 154, 94
- Martell, S. L., Shetrone, M. D., Lucatello, S., et al. 2016, *ApJ*, 825, 146
- Massari, D., Koppelman, H. H., & Helmi, A. 2019, *A&A*, 630, L4
- Mészáros, S., Masseron, T., García-Hernández, D. A., et al. 2020, *MNRAS*, 492, 1641
- Minniti, D., Geisler, D., Alonso-García, J., et al. 2017, *ApJL*, 849, L24
- Nidever, D. L., Holtzman, J. A., Allende Prieto, C., et al. 2015, *AJ*, 150, 173
- Nissen, P. E., & Schuster, W. J. 2010, *A&A*, 511, L10
- Queiroz, A. B. A., Anders, F., Santiago, B. X., et al. 2018, *MNRAS*, 476, 2556
- Queiroz, A. B. A., Anders, F., Chiappini, C., et al. 2020a, *A&A*, 638, A76
- Queiroz, A. B. A., Chiappini, C., Perez-Villegas, A., et al. 2020b, arXiv e-prints, arXiv:2007.12915
- Sanders, J. L., Smith, L., & Evans, N. W. 2019, *MNRAS*, 488, 4552
- Santana, F. A., Beaton, R. L., Covey, K., et al. 2021, *ApJ*, in preparation
- Schiavon, R. P., Zamora, O., Carrera, R., et al. 2017, *MNRAS*, 465, 501
- Shetrone, M., Bizyaev, D., Lawler, J. E., et al. 2015, *ApJS*, 221, 24
- Shetrone, M., Tayar, J., Johnson, J. A., et al. 2019, *ApJ*, 872, 137
- Simpson, J. D. 2018, *MNRAS*, 477, 4565
- Smith, V. V., Bizyaev, D., Cunha, K., et al. 2021, *AJ*, 161, 254
- Vasiliev, E., & Baumgardt, H. 2021, *MNRAS*, 505, 5978
- Wan, Z., Lewis, G. F., Li, T. S., et al. 2020, *Nature*, 583, 768
- Wilson, J. C., Hearty, F. R., Skrutskie, M. F., et al. 2019, *PASP*, 131, 055001
- Zamora, O., García-Hernández, D. A., Allende Prieto, C., et al. 2015, *AJ*, 149, 181
- Zasowski, G., Cohen, R. E., Chojnowski, S. D., et al. 2017, *AJ*, 154, 198